STRUCTURAL ANALYSIS OF BIOLOGICAL MACROMOLECULAR ASSEMBLIES BY ELECTRON MICROSCOPIC TECHNIQUES

Miloslav BOUBLIK*, Valsan MANDIYAN and Santa J. TUMMINIA

Roche Institute of Molecular Biology, Roche Research Center, Nutley, NJ 07110, U.S.A.

Received October 10, 1990
Accepted October 17, 1990

Dedicated to the memory of Professor František Šorm.

The development of high resolution electron microscopic techniques and the introduction of quantitative image analysis has provided a direct basis for studying the structure of biological macromolecules. Apart from the determination of overall morphology, including 3-D image reconstruction, these techniques provide information on the internal architecture of biological macromolecular assemblies, the topography of functional sites, the interactions of their components and elemental microanalysis in situ. Thus, from a mere photographic recording system of the past, electron microscopy has evolved into a high resolution quantitative spectroscopic analytical method.

The structure of biological macromolecules can be studied by a wide range of physico-chemical techniques such as sedimentation analysis, affinity labeling, chemical and enzymatic probing, fluorescent spectroscopy, light scattering, small angle X-ray scattering, neutron diffraction, nuclear magnetic resonance, circular dichroism, Raman spectroscopy, electron microscopy and X-ray crystallography. Most of these techniques possess the capability of providing information on the overall morphology of biomolecular complexes, the topography, conformation, and/or interactions of their components at various levels of resolution. At present, the ultimate method for determining the three-dimensional structure of a macromolecule is considered to be X-ray crystallography because the obtained data reflect details of molecular shape and internal architecture at atomic level. However, the application of X-ray crystallography is limited to specimens in a crystalline state, a condition not always attainable for biological material. In addition, the structure determined from X-ray crystallographic data does not necessarily reflect a conformational state of the investigated molecule in a specific ionic environment. These conditions can be monitored more directly and in a relatively simpler way by some of the newly developed electron microscopic (EM) techniques.[1]

* To whom all correspondence should be addressed.

EXPERIMENTAL

Specimen solutions — general rules. All solutions for high resolution electron microscopic imaging should be prepared from distilled deionized water. Use of quartz-distilled water is recommended but not always mandatory. All chemicals used should be of analytical grade. Sterile conditions should be strictly observed with some specimens (ribosomal RNAs) in all preparative stages. While some of the specimens (viruses) can be deposited in distilled water, others require the presence of salts. In order to preserve the native structure and activity of the specimen and facilitate the correlation of structure with function, buffer composition should be similar to that used in biochemical assays. E.g., for EM of ribosomes the most commonly used buffers contain 10—20 mM Hepes-KOH (or Tris-HCl), pH ~7·6, 50—100 mM KCl (or NH_4Cl), 2—20 mM Mg acetate and 0·5—2·0 mM dithiothreitol or 2-mercaptoethanol. Magnesium ions are of particular importance since a minimal concentration of 2 mM Mg^{2+} is necessary for preserving the native structure of ribosomal subunits and their association into a monosome. In addition, magnesium ions affect the stacking and stability of the bases present in nucleic acids.

Electron microscopy. The most convenient techniques for the direct imaging and analysis of morphological parameters, internal structure and composition of biological macromolecules are conventional transmission electron microscopy (TEM) and scanning transmission electron microscopy (STEM). STEM is, in principle, a transmission EM operating in a scanning mode, however, construction of a dedicated STEM makes it uniquely suited to quantitative structural analyses of biological specimens.[2] The major advantage of the dedicated STEM is the separation of the components that affect resolution and contrast (Fig. 1a). The probe-forming components

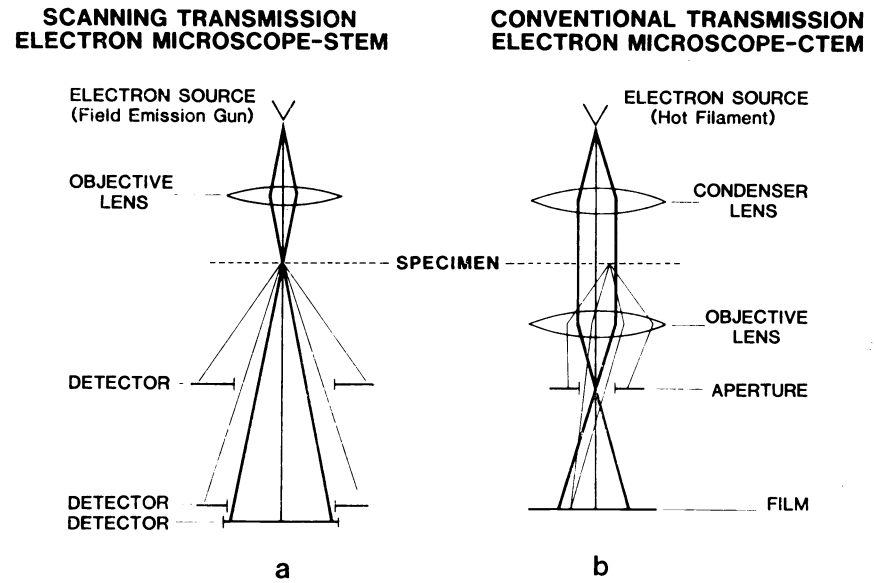

FIG. 1

A comparison of the image-forming system in scanning transmission a and conventional transmission electron microscopes b

(field emission gun, condenser lens, aperture, deflection coils, and objective lens) are all above the specimen, leaving the space below the specimen free for optimal placement of detectors (annular detectors for elastic scattering, energy loss spectrometer for inelastic scattering). Thus, every electron emerging from the specimen can be counted with an appropriate detector to convey information about the specimen volume irradiated at that instant. In the conventional TEM (Fig. 1b) there is only a single imaging channel with a very limited acceptance angle to minimize lens aberrations. Thus, the conventional TEM operated in the dark-field mode can utilize only ~5% of the available elastically scattered, i.e. contrast forming, electrons. To compensate for this loss, the radiation dose in the dark-field TEM for the same signal-to-noise ratio (S/N) must be approximately 20 times higher than in STEM. The superior S/N associated with the STEM annular detector and the high contrast of the dark-field mode make it possible to visualize specimens at a minimal radiation dose and without the necessity of specimen "staining" with heavy metals. The fraction of large-angle elastically scattered electrons is linearly proportional to the mass thickness, thus enabling quantitative measurement of the specimen molecular mass.[2,3] Compared to conventional spectroscopic and hydrodynamic methods applied to the characterization of macromolecular parameters which monitor average values over a total population of particles, STEM has a unique option in the selection and examination of any particular macromolecule in the preparation. Because of the differences in specimen preparation and image processing, the application and potential of both techniques for structural studies of biological macromolecules will be discussed separately.

RESULTS AND DISCUSSION

Transmission Electron Microscopy (TEM)

The extent of fidelity to which an electron micrograph corresponds to the native structure of a specimen depends strongly on both the degree of denaturation during its isolation and on its handling during the preparation for EM imaging. High resolution EM of biological macromolecules is, in general, a demanding task because of their high degree of hydration, low contrast and, in particular, their sensitivity to radiation damage by the beam of electrons at high magnification. Distortion of the specimen by any of the above preparative steps is usually manifested in the loss of fine structural features and specimen mass.

In a typical preparation for high resolution TEM, a specimen (e.g., virus, ribosome, phage, chromatin) in a buffer solution is adsorbed to a thin carbon support film, "stained" for contrast with aqueous uranyl acetate (for air-dried specimens) or "shadowed" with heavy metal (after freeze-drying), and observed in the EM at ~60–120 kV and a direct magnification of ~40,000–120,000×. There are variations in the individual preparative stages,[4,5] e.g., the support carbon film can be treated by a glow-discharge to enhance the specimen adsorption, the specimen can be deposited between two carbon films (sandwich), or the concentration of the uranyl acetate solution can be varied between 0·05% and 2% and result either in negative or positive specimen staining.[5] These variations have a discernible but largely predictable effect on the observed structures. Specimen resolution can be most adversely

affected by the dehydration procedure and radiation damage caused by the specimen's exposure to a relatively high dose of electrons (over 1 000 e/Å^2, depending on the magnification). These two factors are the main sources of artifacts which could lead to misinterpretation of the structural features observed in electron micrographs of stained airdried specimens. An additional limitation of the resolution stems from specimen thickness.

Resolution in the EM depends on both the technical parameters of the microscope and on the nature of the specimen. For an ideal specimen such as a crystalline lattice of gold or carbon, the theoretical resolution of a high performance TEM is close to 1 Å. Obviously, biological specimens are rather distant from the ideal state because of their high hydration, susceptibility to radiation damage and the necessity of staining. In spite of these drawbacks, conventional TEM proved to be an invaluable technique for high resolution visualization of the morphology of biological specimens and the topographical mapping of their components, as demonstrated below in some examples.

Morphology. The imaging of particles invisible in the optical light microscope used to be the primary goal of EM. However, with the progress in the resolution of the EM technique some of the "invisible" specimens, e.g., bacteria, are too big for the observation of their internal ultrastructure and have to be cut into sections. Since the thickness of the specimen drastically reduces the resolution, the specimen sections should be as thin as possible. The effect of specimen thickness on the resolution is demonstrated in a comparison of the morphology of ribosomal particles embedded in the "thin" (~1 000 Å) section of liver tissue (arrows in Fig. 2) and of a free ribosome (~260 Å) (insert in Fig. 2). The image of the free ribosome is at a considerably higher magnification, however, enlargement of the ribosome image in the thin section would just increase its size, not the resolution, and would not reveal the structural details resolved in the image of the free particle.

a) Lipids. Electron micrographs of free lipids in thin sections of a tissue reveal merely structureless circles of various diameters. Structural studies of lipids by EM became of broader interest only after the establishment of the biological activity of some of the lipoprotein complexes[6] and their involvement in active transport across the cell membrane where they form the lipid bilayer. The electron micrograph in Fig. 3 demonstrates a structural form of lipoproteins in solution. These multilayer lipoprotein complexes, called liposomes, were developed for targeted drug delivery in therapeutical treatment.

b) Proteins. Imaging of simple globular proteins with a molecular mass (M) smaller than 50 kDa is below the meaningful resolution power of the conventional TEM. Larger proteins ($M > 50$ kDa) appear in TEM as compact particles such as depicted in Fig. 4. This electron micrograph shows molecules of eukaryotic protein initiation factor, eIF-3, as globules with a diameter of about 100 Å and $M \geqq 400$ kDa. Proteins

FIG. 2

Electron micrograph (TEM) of a thin section of rat liver tissue. Arrows denote ribosomes seen as small electron dense particles attached to the membrane of the endoplasmic reticulum. Inset shows a high resolution electron micrograph of a single free ribosomal particle (80S) consisting of the small (S) and large (L) subunit

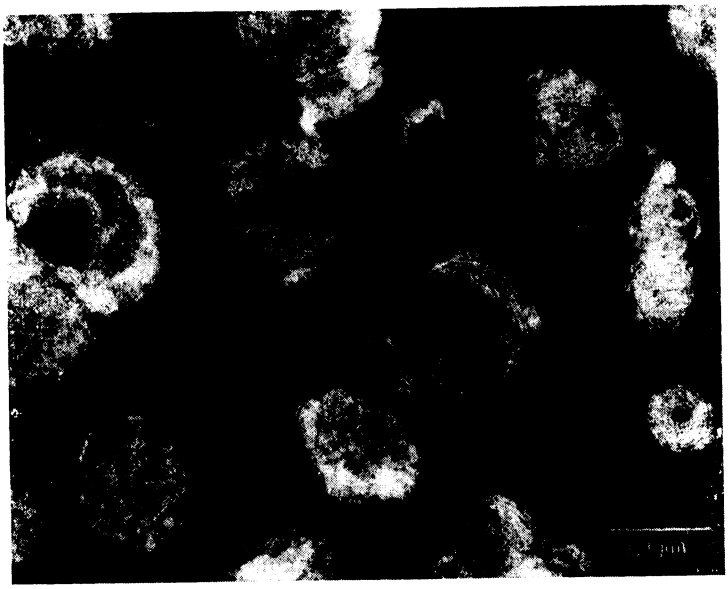

FIG. 3

Electron micrograph (TEM) of multilayer lipoprotein complexes (liposomes) stained with 0·5% uranyl acetate

of these dimensions are often composed of subunits arranged in quaternary structure which can be enhanced by computer image processing, and some proteins, e.g. actin and immunoglobulins, have a characteristic rigid structure which facilitates their imaging. In addition, the typical Y-shape molecules of antibodies (IgG) is utilized in immunoelectron microscopy as a topographical marker (see Fig. 7).

c) Nucleic acids. Conventional TEM lacks both contrast and resolution for the visualization of free nucleic acids in a form suitable for quantitative structural analysis. Spreading of DNA or RNA molecules under denaturing conditions (for length and mass measurements) and contrasting these molecules with heavy metals[7,8] adversely affect their native structure and resolution. These limiting conditions can be overcome by the application of STEM (see Fig. 9).

d) Nucleoprotein complexes. This class encompasses biomolecular assemblies of great diversity in composition and molecular parameters. They can be composed of a single nucleic acid molecule (RNA or DNA) and a few proteins, e.g. viruses, or several different nucleic acids and a large number of proteins, e.g., ribosomes. The mass of these nucleoprotein complexes is in the range of megadaltons (MDa), their dimensions vary from ~100 Å to ~5 000 Å and their shapes can be simple and symmetric or complicated and highly asymmetric. Some examples are represented in Figs 5 and 6. Polio virus particles (Fig. 5a) appear as regular spheres with a diameter of ~280 Å in negatively stained preparations. There is an indication of the

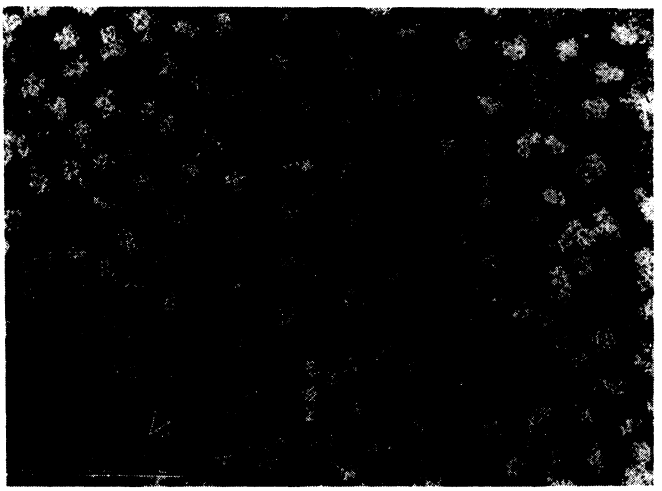

FIG. 4

Electron micrograph (TEM) of initiation factor eIF-3 molecules from rabbit reticulocytes. Arrows point to the molecules which seem to show a quaternary structure of the factor. Fixed with 0·5% glutaraldehyde and stained with 0·5% aqueous uranly acetate. Bar 0·1 μm

icosahedral symmetry of the virion, but capsomeric arrangement cannot be resolved without image processing[9,10] because of their small size. The arrows point to the "empty" viral particles which are missing the RNA genome. Particles of reovirus (Fig. 5b) which belong to the same virus family as polio are considerably larger

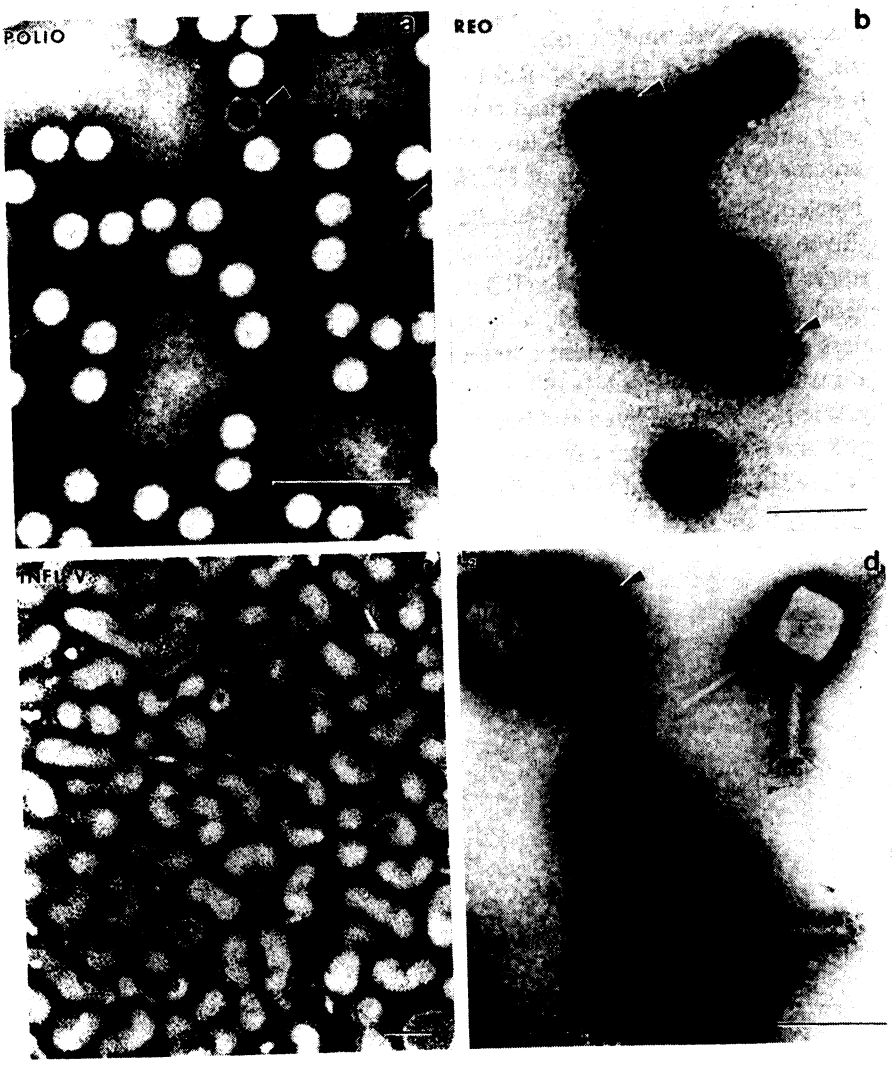

FIG. 5

Electron micrographs (TEM) of a polio virus, b reovirus, c influenza virus, and d bacteriophage T_2, stained with 0·5% aqueous uranyl acetate. Arrows point to the "empty" particles. Bar in each figure represents 0·1 μm

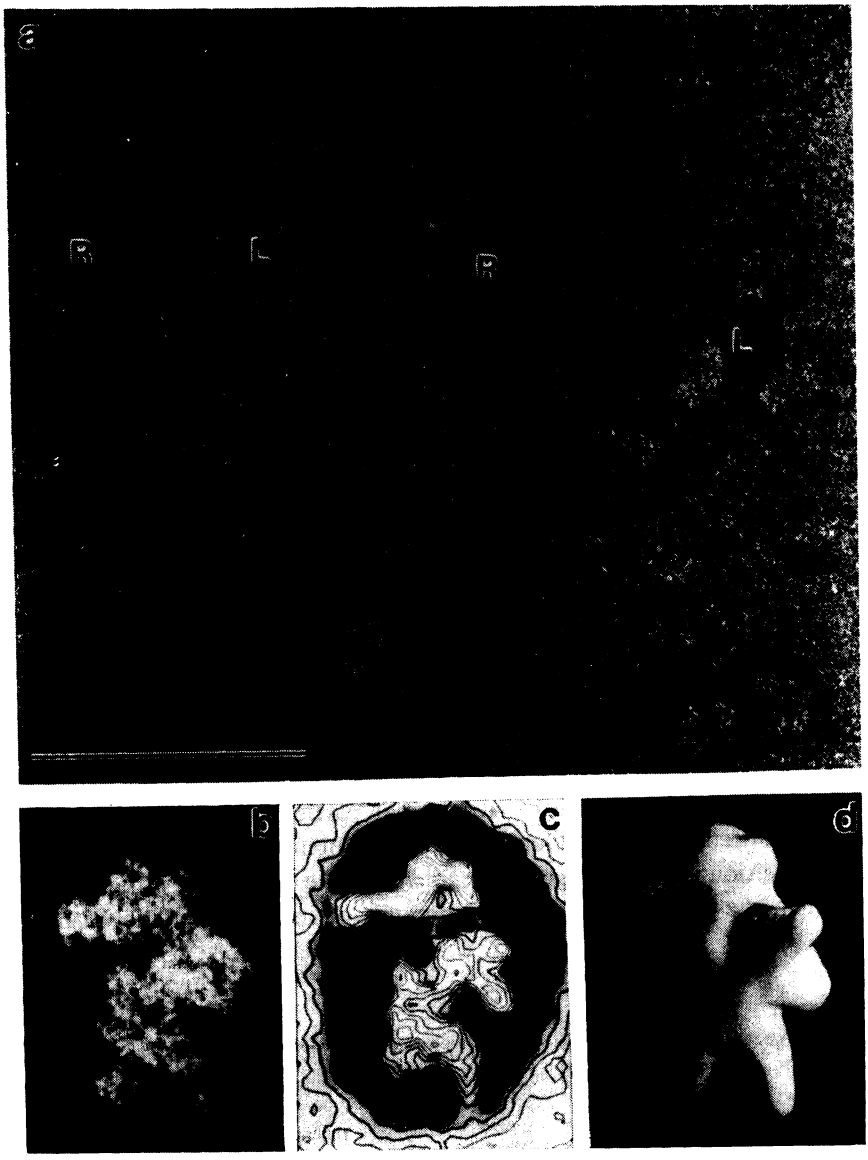

FIG. 6

a Electron micrograph of eukaryotic 40S ribosomal subunits from HeLa cells, stained with 0·5% aqueous uranyl acetate. Subunits show preferential orientation for two lateral views denoted as R (right) and L (left). Bar 0·1 μm. Gallery shows b highly enlarged electron micrograph of 40S subunit in the L view, c computer processed images of about fifty subunits in the view corresponding to b, and d 3-D model of a eukaryotic 40S ribosomal subunit

(>700 Å in diameter) and have the capsomeric structure clearly visible. Influenza viruses (Fig. 5c) have irregular shapes with an average size of ~1 000 Å and an envelope decorated with spikes which appear as a "fringe" surrounding an electron--lucent center. Beneath the spike layer is a lipid-containing envelope enclosing a matrix protein and a nucleocapsid formed of protein and single stranded RNA. The bizarre construction of bacteriophage T_2 (Fig. 5d) enables the phage to inject its genome into the host bacteria.

An example of a nucleoprotein particle which possesses a highly complex and asymmetric structure is given in Fig. 6. This electron micrograph shows a field of small eukaryotic 40S ribosomal subunits from HeLa cells (Fig. 6a). The subunits can be obtained by dissociation of the 80S monosomes (such as that shown in the inset in Fig. 2) by lowering the Mg^{2+} concentration in the buffer solution. The subunits have a strong preferential orientation for lateral views (right (R) or left (L)). The images of individual particles (Fig. 6b) can be aligned and processed by correspondence analysis[9-11] (Fig. 6c) and used as a basis for the proposal of a 3-D model of the small eukaryotic ribosomal subunit (Fig. 6d).

Topography. Apart from the determination of the overall morphology, molecular parameters and ultrastructure of biomolecular assemblies, TEM can be applied to the in situ localization of their macromolecular components and the mapping of functional sites.

The standard technique used to localize individual proteins, segments of nucleic acids and functional sites in situ, is immunoelectron microscopy (IEM). This technique, originally developed for ribosomes[12], has been recently reviewed in detail by Stöffler-Meilicke and Stöffler[13]. Ribosomal particles are incubated with antibodies (IgG) specific for individual ribosomal proteins. The binding site of IgG marks the position of the antigen, a segment of the particular protein or rRNA against which the antibody was raised. Because of its characteristic Y-shape, the

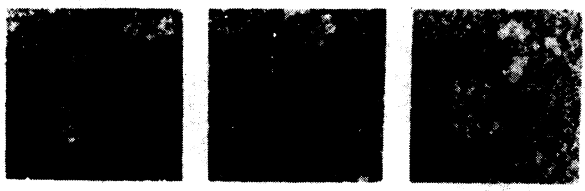

FIG. 7

Electron micrographs (TEM) of the *E. coli* 30S ribosomal subunit labeled with an antibody (IgG) attached to the 3'end of the tRNA on the subunit. Magnification × 620,000

antibody can be resolved directly without additional electron densed markers such as colloidal gold or ferritin. The example in Fig. 7, obtained by a combination of IEM and affinity labeling[14], demonstrates the localization of the decoding region of the *E. coli* ribosome to the "cleft" of the small subunit.

An alternative approach to the mapping of functional sites by conventional TEM is by localizing the area of stain exclusion due to the local changes in conformation and/or mass distribution. This technique is more demanding than IEM and requires the statistical evaluation of particles in corresponding views by single-particle image averaging technique[15] similar to that described for the model proposed of the 40S subunit (Fig. 6).

A summary of the application of TEM for structural studies on biomolecular assemblies is demonstrated in Fig. 8 on 30S *E. coli* ribosomal subunits.

Scanning Transmission Electron Microscopy (STEM)

The advantages of STEM for application to sensitive biological material were already emphasized in the Experimental Procedures. Specimen preparation for STEM differs from the TEM technique mainly in the elimination of staining and the substitution of air-drying by freezedrying. Both of these steps are possible because of the high (>80%) collection efficiency of scattered electrons in the STEM dark-field mode. Also, the applied electron dose is about 1 e/Å^2 at a magnification of 50,000× and 30 e/Å^2 at 250,000×, which is about two orders of magnitude lower than in

FIG. 8

Model of the *E. coli* 30S subunit[16] shows topographically identified 16S rRNA sites: C_{1400}, the ribosomal decoding site[17], A_{1542}, the 3'end of 16S rRNA (ref.[18]), modified bases $m_2^6A_{1518}$ (ref.[19]), m^7G_{527} (ref.[20]), A_1, the 5'end of 16 S rRNA (ref.[21]), puromycin (PM) crosslinking site[22], the mRNA binding domain[23] and the location of some ribosomal proteins[13]

TEM at the same magnification. Specimens prepared in this manner are free of the main resolution-limiting effects inherent in conventional TEM, i.e., staining, distortion by air-drying, and radiation damage. With the elimination of staining it becomes possible to relate image intensity to the local projected mass of the specimen, and thus to obtain, apart from the morphology, quantitative data on the molecular mass and mass distribution within a single macromolecule, mass/length ratio (M/L), number of strands (n) in the conformation of a nucleic acid, and to calculate the radius of gyration (R_G), a parameter closely related to the 3-D structure of the investigated specimen.[4]

Morphology and mass. Visualization of biomolecular assemblies under conditions in which they display native conformations or conformations reflecting the ambient ionic conditions has become possible only after the application of STEM. The difference in the potential of TEM and STEM techniques for structural studies becomes evident from the comparison of the images of nucleic acids. The electron micrograph in Fig. 9a is an example of an image of 23S rRNA molecules obtained by TEM with the routinely used benzylalkylammonium chloride (BAC) spreading technique[8]. The obvious difference in the length, thickness and structural pattern of the 23S rRNA molecules in the TEM image (Fig. 9a) and in the STEM image (Fig. 9b) reflects the mode of specimen deposition on the support carbon film. 23S rRNA (Fig. 9a) spread on water hypophase and stretched under denaturing conditions appears as a single thick filament with the length of ~10,000 Å. This value corresponds to the number of nucleotides in 23S rRNA (2 904) in its fully extended form. Deposition of BAC and shadowing by the evaporation of tungsten, for contrast enhancement, covers the fine structures resolvable on the STEM images of unstained freeze-dried RNA molecules (Fig. 9b). Under the non-denaturing conditions used in the STEM deposition technique, the length of the 23S rRNA molecules in Fig. 9b is ~2 500 Å. The "shortening" of the 23S rRNA molecule is expected because of the preservation of its native secondary structure which consists of intramolecular double-stranded stems (about 60–70% of nucleotides in native rRNAs form base pairs) alternating with single-stranded loops of various size. The total molecular mass of 23S rRNA as determined by STEM is 1 210 kD ± 50 kD, in reasonable agreement with the theoretical value of 1 050 kD calculated from the established composition of 23S rRNA. Given the linearity of the STEM imaging process, direct measurements of particle mass is relatively straightforward and has been described in detail elsewhere[3,4,5].

Linear density and the apparent number of strands. Determination of these parameters can be applied only to highly extended structures such as nucleic acids, filamentous or rod-like viruses, flagellae and/or tubular proteins. Fig. 9c serves as an example for the calculation of M/L on ribosomal RNA (refs[24,25]). The M/L of the 23S rRNA molecules vary in different segments (Fig. 9c, Table I), but the

average value of M/L for these molecules is 480 Da/Å. This value is about four times higher than that expected for single-stranded RNA (125 Da/Å) which is derived from a 2·8 Å axial rise per residue for A-RNA double helices. These data indicate a close association of four-stranded or two double-stranded polynucleotide strands in the main structural backbone of the observed molecules. Determination of a total molecule length of 2 500 Å, which is ~1/4 of that in the fully extended state, supports this explanation. However, at present there is no direct evidence on the mutual orientation of the nucleotide strands. They may form coaxial helixes and/or be a mere combination of double and single strands in a side-by-side position. Asymmetric

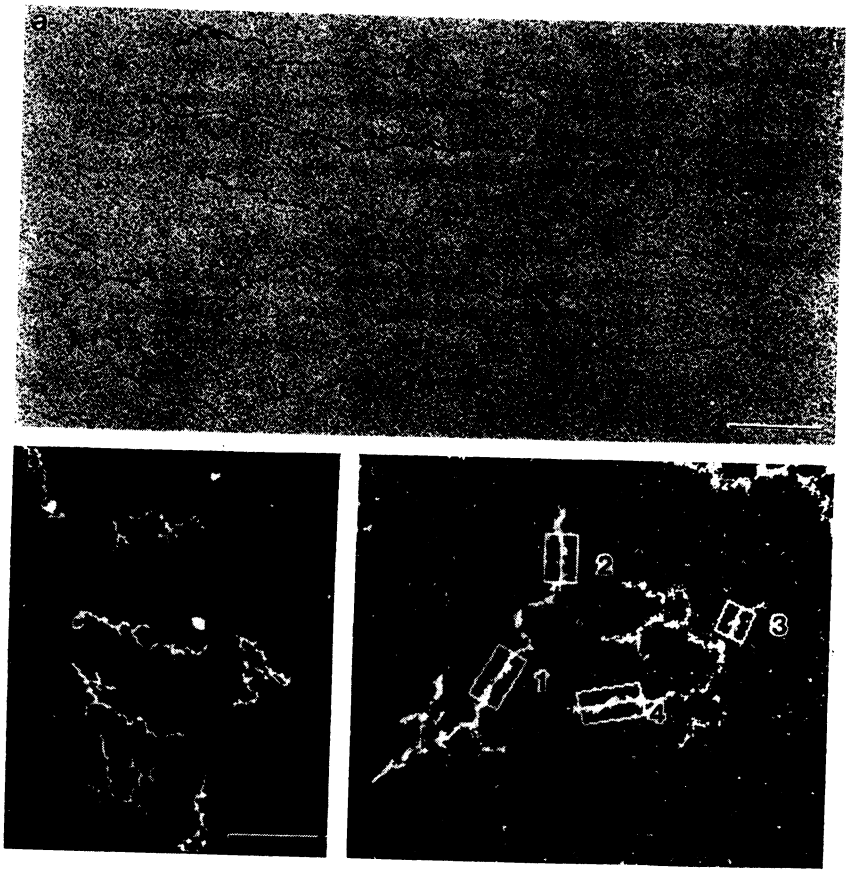

FIG. 9

Electron micrograph of *E. coli* 23S rRNA obtained by a conventional TEM and BAC-monolayer technique[8], air-dried and shadowed with Pt-Pd; b scanning transmission EM, unstained and freeze-dried. In both cases, samples were deposited from water. c Enlarged image of b with segments 1—4 used for the determination of linear density (see Table I). Bar represents 0·1 μm

distribution of the branched regions can be used for alignment of the molecules, determination of their polarity and the proposal of a structural model[26].

Conformational transitions and radii of gyration. Biomolecular assemblies are typical polyelectrolytes and their conformation is dependent upon the ambient ionic conditions. Conformational transitions due to changes in buffer conditions are demonstrated in electron micrographs in Fig. 10 on an example of *E. coli* 16S rRNA. The conformational changes can be monitored visually, or more precisely by calculation of radius of gyration (R_G). In water (Fig. 10a) the RNA molecules are quite extended ($R_G = 556 \pm 67$), in low ionic strength (up to 0·1 mol l^{-1}, pH 7·6 – Fig. 10b) they still exist in an extended, loosely coiled form ($R_G = 142 \pm 22$), while in higher ionic strength (~0·3 mol l^{-1}, pH 7·6 – Fig. 10c) the molecules undergo tighter coiling ($R_G = 115 \pm 16$). Under high salt conditions it becomes difficult to monitor the individual segments of the molecule and to determine the M/L. However, from the overall shapes of individual rRNA molecules and from the mass distribution in their digitized images, it is possible to establish the center of gravity and calculate the R_G (Table II).

Determination of the R_G facilitates a comparison between the structural data obtained by electron microscopy and by other techniques in which the specimens are monitored in the fully hydrated state and under controlled buffer conditions. The R_G values of ribosomal subunits and rRNAs determined by STEM (Table II) are in good agreement with the published values of R_G obtained by X-ray scattering[27].

Interactions of nucleic acids with proteins. Protein-free deposition of rRNAs under non-denaturing conditions[24,25] makes it possible to visualize and analyze nucleic acid-protein interactions[28] and, ultimately, the complete assembly process of a nucleoprotein complex or cellular organelle. The major criteria for monitoring

TABLE I

Length (L), mass (M), linear density (M/L) and estimated number of nucleotide strands (n) in arbitrary segments of 23S *E. coli* rRNA in water

Segment[a]	L, Å	M, kDa	M/L, Da/Å	n
1	320	479	1 464	11
2	243	110	455	4
3	184	62	335	3
4	251	109	434	4

[a] See Fig. 9.

TABLE II

Molecular mass (M in kDa) and radii of gyration (R_G in Å) of *E. coli* 16S and 23S rRNA (in various buffer conditions) and of the 30S and 50S ribosomal subunits calculated from STEM data

Solution	M^a	$M \pm$ S.D.	$R_G \pm$ S.D.
16S rRNA in water	550	551 ± 22	305 ± 50
23S rRNA in water	1 050	1 210 ± 50	566 ± 67
16S rRNA in low μ^b	—	—	114 ± 20
23S rRNA in low μ^b	—	—	142 ± 22
16S rRNA in high μ^b	—	—	80 ± 10
23S rRNA in high μ^b	—	—	115 ± 16
30S *E. coli* subunit	900	872 ± 41	70 ± 40
50S *E. coli* subunit	1 650	1 624 ± 7	69 ± 2

[a] Theoretical values calculated from the established composition; [b] μ ionic strength.

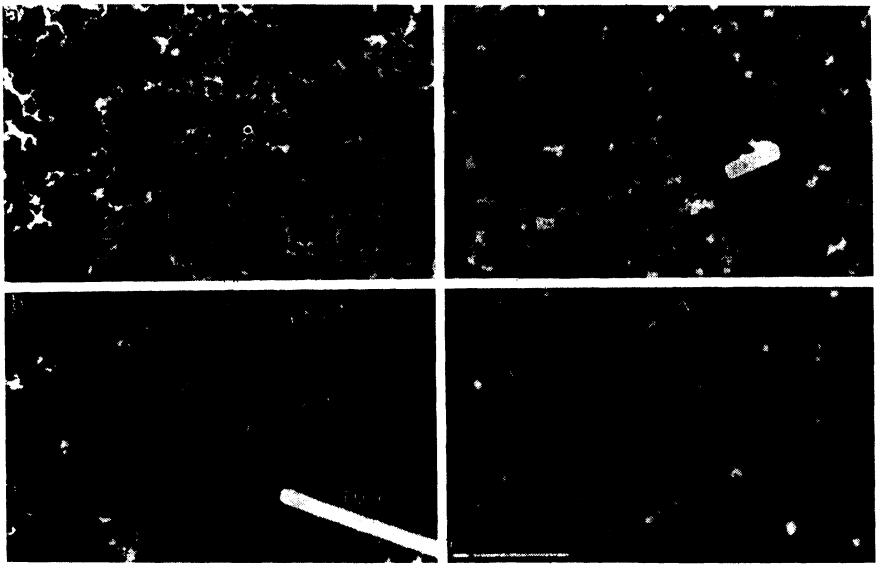

FIG. 10

Electron micrographs (STEM) of *E. coli* 16S rRNA, unstained, freeze-dried, and deposited from a water; b—c buffers of increasing ionic strength; d STEM image of 16S rRNA associated with the primary binding proteins. TMV denotes molecules of tobacco mosaic virus used as a size and stability marker. Bar represents 0·1 μm

these interactions are differences in mass, shape, and mass distribution reflected in the values of R_G.

Imaging of RNA–protein interactions is demonstrated in Fig. 10d using as an example 16S rRNA from *E. coli* associated with the six primary binding ribosomal proteins (S4, S8, S15, S20, S17 and S7). The complex of 16S rRNA with these proteins has been prepared as described[28]. The structure of protein-free 16S rRNA (Figure 10a) in the corresponding buffer conditions is characterized by a loose coil with a mass of 551 ± 22 kD and an R_G value of 114 ± 20 Å, while complexes of 16S rRNA with the six bound proteins (Figure 10b) differ from free 16S rRNA by a corresponding increase in mass (M = 625 ± 25 kD) and by shape and mass distribution as characterized by an R_G value of 108 ± 11 Å.

Topography. Both labeling techniques described for TEM, immunoelectron microscopy and "stain" exclusion can be used for topographical mapping in STEM. Elimination of staining makes it feasible to quantitatively evaluate the local changes in the mass of a biomolecular assembly due to the binding or depletion of another macromolecule, e.g., protein (enzyme, factor, immunoglobulin) or nucleic acid (tRNA, mRNA). This approach is obviously more precise than visual evidence. Elimination of heavy metals allows the use of heavy atoms as markers. A new class of these compounds, denoted as "clusters"[29], which are small organic complexes with regularly spaced heavy atoms (Au, W, Pt), is of particular interest. Cluster compounds can be attached to specific groups (amino, sulfhydryl) on proteins or

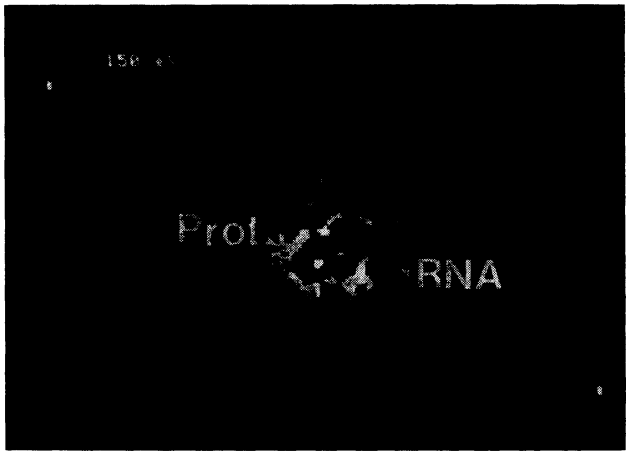

FIG. 11

Example of an application of the electron energy loss spectroscopic (EELS) technique for the in situ determination of the protein and rRNA protein moiety distribution in the *E. coli* 50S ribosomal subunit

nucleic acids. Resolution of this labeling technique[30] is about 10 Å. Finally, the application of spectrometers in cobmination with STEM makes it possible to determine elemental composition in situ which can be used to determine the localization of an RNA molecule within a virus or ribosome or to discriminate between the protein and RNA moiety[31] as shown in Fig. 11.

FUTURE TRENDS

Electron microscopic techniques will continue to play a significant role in studies on the structure–function relationship of biological macromolecules. The emphasis will be on improving resolution and objective quantitative analysis of the EM data. This trend should be pursued at the level of specimen, instrumentation and image processing.

At the specimen level, the major effort will be directed towards the preservation of its native structure. The most promising and most challenging approach is the imaging of unstained frozen hydrated specimens embedded in thin film of vitreous ice. In topographical mapping of macromolecular components and functional domains, substantial progress both in resolution and specificity is expected from the application of the cluster compounds.

In the area of instrumentation, the resolution should be improved by reducing the radiation dose and by introducing a broader spectrum of specialized high performance spectroscopic techniques, e.g. electron energy loss spectroscopy (EELS) providing specific and quantitative data on specimen mass and element composition and distribution in situ.

The availability of dedicated computer programs for the analysis of high resolution electron micrographs will ensure an objective evaluation of EM data and improve the resolution of three-dimensional reconstruction and of models proposed for biological macromolecules from their EM images.

The authors gratefully acknowledge extensive collaboration, contributions and discussions in computer image processing with Drs J. Frank, T. Wagenknecht, M. Radermacher and A. Verschoor from the Wadsworth Laboratory in Albany, N.Y., Drs J. S. Wall and J. F. Hainfeld from the Brookhaven STEM Biotechnology Resource, and the excellent assistance of W. Hellmann from our laboratory.

REFERENCES

1. Peachey L. D., Williams D. B. (Eds): *Proceedings of the XIIth International Congress for Electron Microscopy*. San Francisco Press Inc., Seattle 1988.
2. Wall J. S. in: *Introduction to Analytical Electron Microscopy* (J. J. Hren, J. I. Goldstein and D. C. Joy, Eds), p. 332. Plenum, New York 1979.
3. Wall J. S., Hainfeld J. F.: Ann. Rev. Biophys. Chem. *15*, 355 (1986).
4. Boublik M., Oostergetel G. T., Mandiyan V., Hainfeld J. F., Wall J. S.: Methods Enzymol. *164*, 49 (1988).

5. Boublik M. in: *Ribosomes and Protein Synthesis: A Practical Approach* (G. Spedding, Ed.), p. 273. Oxford University Press, Oxford 1990.
6. Scanu A. M., Landsberger F. R. (Eds): *Lipoprotein Structure in Annals of the New York Academy of Sciences*, Vol. 348. New York Academy of Sciences, New York 1980.
7. Kleinschmidt A. K.: Methods Enzymol., B *12* 361 (1968).
8. Sogo J. M., Rodeno P., Koller T., Vinuela E., Salas M.: Nucleic Acids Res. *7*, 107 (1979).
9. Frank J., Verschoor A., Boublik M.: Science *214*, 1353 (1981).
10. Frank J., Radermacher M., Wagenknecth T., Verschoor A. in: *Annals of the New York Academy of Sciences*, Vol. 483, p. 361. New York Academy of Sciences, New York 1986.
11. Verschoor A., Frank J., Radermacher M., Wagenknecht T., Boublik M.: J. Mol. Biol. *178*, 677 (1984).
12. Wabl M. R.: J. Mol. Biol. *84*, 241 (1974).
13. Stöffler-Meilicke M., Stöffler G.: Methods Enzymol. *164*, 503 (1988).
14. Keren-Zur M., Boublik M., Ofengand J.: Proc. Natl. Acad. Sci. U.S.A. *83*, 275 (1979).
15. Wagenknecht T., Frank J., Boublik M., Nurse J., Ofengand J.: J. Mol. Biol. *203*, 753 (1988).
16. Boublik M., Robakis N., Hellmann W., Wall J. S.: Eur. J. Cell Biol. *27*, 177 (1982).
17. Gornicki P., Nurse K., Hellmann W., Boublik M., Ofengand J.: J. Biol. Chem. *259*, 10493 (1984).
18. Olson H. M., Glitz D. G.: Proc. Natl. Acad. Sci. U.S.A. *76*, 3769 (1979).
19. Politz S. M., Glitz D. G.: Proc. Natl. Acad. Sci. U.S.A. *74*, 1468 (1955).
20. Trempe M. R., Ohgi K., Glitz D. G.: J. Biol. Chem. *257*, 9822 (1982).
21. Mochalova L. V., Shatsky I. N., Bogdanov A. A., Vasiliev V. D.: J. Mol. Biol. *159*, 637 (1982).
22. Olson H. M., Grant P. G., Glitz D. G., Cooperman B. S.: Proc. Natl. Acad. Sci. U.S.A. *77*, 890 (1980).
23. Stöffler G., Stöffler-Meilicke M. in: *International Cell Biology* (H. G. Schweiger, Ed.), p. 93. Springer-Verlag, New York 1980/81.
24. Mandiyan V., Hainfeld J. F., Wall J. S., Boublik M.: FEBS Lett. *236*, 340 (1988).
25. Mandiyan V., Tumminia S., Wall J. S., Boublik M.: Arch. Biochem. Biophys. *276*, 299 (1990).
26. Oostergetel G. T., Wall J. S., Hainfeld J. F., Boublik M.: Proc. Natl. Acad. Sci. U.S.A. *82*, 5598 (1985).
27. Hill W. E., Thompson J. D., Anderegg J. W.: J. Mol. Biol. *44*, 89 (1969).
28. Mandiyan V., Wall J. S., Hainfeld J. F., Boublik M.: J. Mol. Biol. *210*, 323 (1989).
29. Wall J. S., Hainfeld J. F., Bartlett P. A., Singer S. J.: Ultramicroscopy *8*, 397 (1982).
30. Hainfeld J. F.: Science *236*, 450 (1987).
31. Boublik M., Oostergetel G. T., Joy D. C., Wall J. S., Hainfeld J. F., Frankland B., Ottensmeyer P. F. in: *Annals of the New York Academy of Sciences*, Vol. 463, p. 168. New York Academy of Sciences, New York 1986.